Integrated predictive modeling simulations of the Mega-Amp Spherical Tokamak

Canh N. Nguyen, Glenn Bateman, Arnold H. Kritz, Robert Akers, Calum Byrom et al.

Citation: Phys. Plasmas **9**, 3930 (2002); doi: 10.1063/1.1498836
View online: http://dx.doi.org/10.1063/1.1498836
View Table of Contents: http://pop.aip.org/resource/1/PHPAEN/v9/i9
Published by the American Institute of Physics.

Integrated predictive modeling simulations of the Mega-Amp Spherical Tokamak

Canh N. Nguyen, Glenn Bateman, and Arnold H. Kritz
Department of Physics, Lehigh University, 16 Memorial Drive East, Bethlehem, Pennsylvania 18015

Robert Akers, Calum Byrom,[a] Alan Sykes, and the MAST Team
EURATOM/UKAEA Fusion Association, Culham Science Centre, Abingdon, Oxfordshire OX14 3DB, United Kingdom

(Received 18 January 2002; accepted 13 June 2002)

Integrated predictive modeling simulations are carried out using the BALDUR transport code [Singer *et al.*, Comput. Phys. Commun. **49**, 275 (1982)] for high confinement mode (*H*-mode) and low confinement mode (*L*-mode) discharges in the Mega-Amp Spherical Tokamak (MAST) [Sykes *et al.*, Phys. Plasmas **8**, 2101 (2001)]. Simulation results, obtained using either the Multi-Mode transport model (MMM95) or, alternatively, the mixed-Bohm/gyro-Bohm transport model, are compared with experimental data. In addition to the anomalous transport, neoclassical transport is included in the simulations and the ion thermal diffusivity in the inner third of the plasma is found to be predominantly neoclassical. The sawtooth oscillations in the simulations radially spread the neutral beam injection heating profiles across a broad sawtooth mixing region. The broad sawtooth oscillations also flatten the central temperature and electron density profiles. Simulation results for the electron temperature and density profiles are compared with experimental data to test the applicability of these models and the BALDUR integrated modeling code in the limit of low aspect ratio toroidal plasmas. © *2002 American Institute of Physics.* [DOI: 10.1063/1.1498836]

I. INTRODUCTION

One objective of the Mega-Amp Spherical Tokamak (MAST) experiment[1,2] is to extend the understanding of tokamak physics to the low aspect ratio regime in order to investigate the potential of the spherical tokamak concept as a fusion power plant. To develop an understanding of the physics explored with the MAST experiments, it is desirable to be able to predict the density and temperature profiles for electrons and ions. Simulations that yield these profiles are the focus of this paper.

The BALDUR integrated predictive transport code[3] has been used to predict temperature and density profiles in conventional tokamaks and the results of these predictions have been compared with experimental data.[4,5] An objective of this paper is to compare predictions for the electron temperature and density profiles obtained using the BALDUR code with experimental data from the MAST experiment in order to test the low aspect ratio limit of the applicability of the models used in the code for thermal and particle transport, as well as plasma equilibrium, thermal and particle sources and sinks, and large scale instabilities. The ion temperature profile was not measured in this experiment and, thus, the simulation of the ion temperature profile cannot be compared with the corresponding experimental data. The central ion temperature, however, which was measured, acts as a calibration point for the simulated ion temperature profile.

It should be noted that the BALDUR integrated modeling simulations have an internal self-consistency that is somewhat independent of the experiment. Inferences made from simulations are logically different from inferences made from experimental data. Thus, even when the inferences coincide numerically, they remain logically different. When we refer to thermal diffusivity, for example, we are referring to the thermal diffusivity computed in the simulation and not necessarily the thermal diffusivity that would be inferred directly from the experiment. When we indicate, for example, that neoclassical diffusion dominates in the central third of the plasma, we mean that neoclassical diffusion dominates in the central third of the simulated plasma. When we note that particles and energy are not lost from the plasma as a direct result of sawtooth crashes, we mean that the sawtooth model that is used in our simulations does not produce a direct loss of particles and energy during each sawtooth crash. In each case, we are referring to the results of our simulations. Once each simulation is set up, the only further contact with experimental data is the comparison that is made with the measured temperature and density profiles at particular diagnostic times.

In this paper, we simulate MAST discharges 2700, a high confinement mode (*H*-mode) discharge, and 2701, a low confinement mode (*L*-mode) discharge. A description of these discharges and the methods used to simulate them are described in Sec. II. The results of the simulations are described in Sec. III and summarized in Sec. IV.

II. BALDUR SIMULATIONS

The BALDUR code computes the evolution of plasma profiles using time-dependent boundary conditions. Transport

[a]Also at University of Manchester Institute of Science and Technology, Manchester, UK.

models available in the BALDUR code include the Multi-Mode model (MMM95) and the mixed-Bohm/gyro-Bohm (mB/gB) model (used in the JETTO code[6]). The mB/gB model is an empirical model that consists of the sum of terms with Bohm and gyro-Bohm scaling.[5] The MMM95 model contains a linear combination of theory-based transport models consisting of the Weiland model for ion temperature gradient and trapped electron drift modes, the Guzdar–Drake model for the drift resistive ballooning mode, and a contribution from the kinetic ballooning mode.[7]

To complete the transport model, neoclassical transport is added to the mB/gB and to the MMM95 anomalous transport models. Based on previous experience with the START low aspect ratio tokamak,[8] it was anticipated that neoclassical transport would play a significant role in the MAST simulations being considered in this paper. Neoclassical ion thermal transport is computed using either the Chang–Hinton 1986 neoclassical model[9] or, alternatively, NCLASS.[10] In NCLASS all the channels of transport are computed, including thermal and particle for ions, electrons, and impurities. When the Chang–Hinton model is used in the BALDUR code to calculate the neoclassical ion thermal diffusivity, the charged particle neoclassical transport is given by Hawryluk, Suckewer, and Hirshman.[11] Note that the derivation of the Chang–Hinton theory is intended to apply to low aspect ratio tokamaks, but the implementation of some of the flux surface averages uses the aspect ratio approximations described in the 1986 Chang–Hinton paper.[9]

Both the *H*-mode and *L*-mode MAST discharges considered in this paper have nominally the same plasma parameters for plasma size, shape, current, magnetic field, and heating power. The plasma parameters used in the simulations of the *H*-mode and *L*-mode discharges are listed in Table I. There are several major differences between these two discharges. First, the line-averaged electron density in the *H*-mode discharge is approximately 60% higher than that of the *L*-mode by the end of the auxiliary heating stage at 250 ms, even though the line averaged densities were nearly the same during the transition from *L*-mode to *H*-mode earlier in the discharge. Second, the edge to line electron density ratio is 0.7 for the *H*-mode discharge while it is 0.3 for the *L*-mode discharge. Finally, the boundary conditions for the temperature and density are different for the two discharges.

TABLE I. Plasma parameters used in BALDUR simulations of MAST discharge 2700 (*H*-mode) and discharge 2701 (*L*-mode).

Discharge	2700	2701
Type	*H*-mode	*L*-mode
Major radius	0.87 m	0.85 m
Minor radius	0.51 m	0.53 m
Elongation	1.8	1.8
Triangularity	0.4	0.4
Toroidal field	0.4 T	0.4 T
Toroidal current	0.5 MA	0.5 MA
P_{NBI}	526 kW	523 kW
$\overline{n_e}$ (10^{19} m^{-3})	2.07	1.25
$n_{\mathrm{edge}}/\overline{n_e}$	0.7	0.3
Edge Z_{eff}	2.0	2.0
Plasma	Deuterium	Deuterium
Impurity	Carbon	Carbon
Diagnostic time (s)	250 ms	250 ms

In simulations of *L*-mode plasmas, the density and temperature at the edge of the simulation are taken from the outermost experimental data point. In simulations of *H*-mode plasmas, the density and temperature at the edge of the simulation are taken from the experimentally measured values at the top of the *H*-mode pedestal. In particular, experimental data points from the inboard edge of the plasma are used in these simulations of MAST. When there is significant uncertainty indicated by a scatter in the data points, multiple simulations are carried out, as described in Sec. III, to explore the sensitivity of the simulated profiles to this uncertainty.

Neutral beam injection (NBI) was used as the auxilary heating in the discharges considered. Approximately 530 kW of NBI heating power was applied from 50 to 250 ms. These discharges used deuterium gas for the initial fill and hydrogen gas injected at 26.5 keV (tangential co-injection). About 76% of the neutral beam power was deposited at full energy, 18% at one-half energy, and 6% at one-third energy. The neutral beam is injected at a 0.7 m tangency radius.

Carbon is assumed to be the dominant impurity species in the simulations. The impurity density at the boundary is specified to be carbon with a concentration that produces $Z_{\mathrm{eff}}=2$ at the boundary. The BALDUR code calculates the evolution of the impurity profiles. The radiated power is assumed to be 20% of the total heating power.

Each simulation starts at 10 ms, during the Ohmic phase of the discharge. Neutral beam injection starts at 50 ms and the transition to *H*-mode, which is controlled by an increase in the boundary temperatures and densities in the *H*-mode discharge, occurs at 220 ms. Profiles are compared with experimental data at 250 ms. Since the profiles are not available at any time other than 250 ms, the initial profiles are taken to be a parabola raised to a power. Simulations were carried out in which the shape and magnitude of the initial profiles were varied. It was found that the final profiles at 250 ms are independent of the shape and magnitude of the initial profiles that were prescribed at 10 ms.

III. SIMULATION RESULTS

The middle and the bottom panels of Fig. 1 show a comparison between the BALDUR simulations and the measured electron temperature and density profiles as a function of major radius for the *L*-mode discharge (2701). The predicted ion temperature profile is shown in the top panel, but the experimental data point indicates only the core weighted ion temperature that was measured using a neutral particle analyzer on loan from the Princeton Plasma Physics Laboratory. There are two profiles shown for each model in each panel. The profiles with the higher central temperature and electron density correspond to the time just before a sawtooth crash, while the profiles with the somewhat flatter lower central temperature and density correspond to the time just after a sawtooth crash. The label NCLASS in Fig. 1 denotes that the NCLASS model (in contrast with Chang–Hinton) has been used to calculate the neoclassical transport as a part of the total transport.

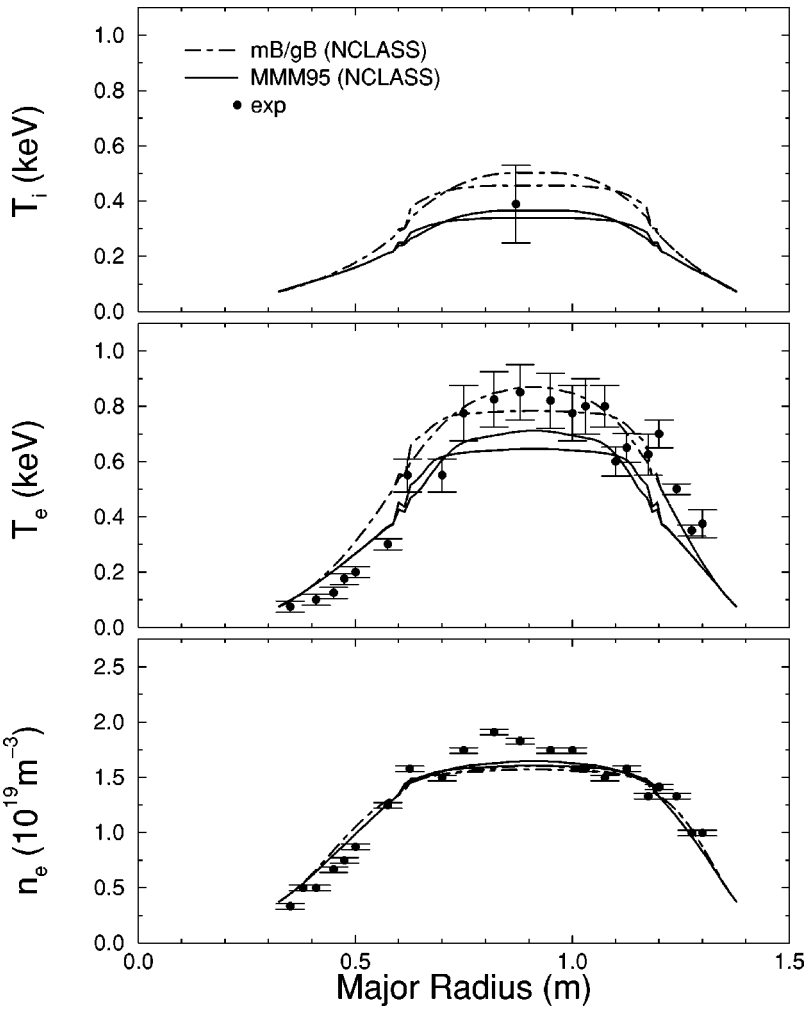

FIG. 1. Ion temperature, electron temperature, and electron density, before and after a sawtooth crash, as a function of major radius for MAST discharge 2701 (L-mode) at 250 ms. Results obtained from a simulation using the mB/gB model are shown with a dashed curve while results obtained using the MMM95 model are shown with a solid curve. For each transport model the profile with the higher central temperature is the profile prior to the sawtooth crash. Experimental data are plotted as closed circles with error bars. NCLASS is used for the neoclassical transport.

The sawtooth periods in the simulations are determined by the Park–Monticello model.[12] The sawtooth periods predicted by this model were found to be less than 5 ms, compared with the 20 ms sawtooth periods observed in the experiment. The frequent sawtooth oscillations are found to cause a fluctuation of less than 15% in the central electron temperature. For example, in the simulation of the L-mode discharge, the central electron temperature varies between 0.78 and 0.86 keV for the mB/gB model over a 4 ms sawtooth period during NBI heating. When the sawtooth period in the simulation is extended to 20 ms, the difference in the central electron temperature before and after a sawtooth crash is approximately four times larger and ranges from 0.7 to 1.0 keV. Sawtooth oscillations have the effect of flattening the temperature and density profiles over a mixing radius that extends over about half the plasma radius in these simulations. Note that the ''mixing radius'' is the radius within which sawtooth mixing occurs. The mixing radius is normally larger than the radius of the $q=1$ surface and larger than the ''inversion radius.''

The sawtooth model used in these simulations mixes the density, thermal energy density, and fast ions within the sawtooth mixing region. Sawtooth crashes have no direct effect on the plasma outside the sawtooth mixing region. In particular, particles and energy are not ejected from the plasma as the direct result of sawtooth crashes according to this model. However, each sawtooth crash results in a large heat and particle pulse that propagates rapidly through the plasma outside the sawtooth mixing region because the heat and particle fluxes computed by the transport models that we use in these simulations are nonlinear functions of the temperature and density gradients. Through this indirect effect, sawtooth crashes can degrade plasma confinement.

For the H-mode discharge (2700), the comparison between BALDUR simulations and measured electron temperature and density profiles is shown in Fig. 2. The Thomson scattering electron temperature profile was taken immediately after a large ELM, which may account for some distortion in the measured electron temperature profile data.

Note, the edge temperature is higher and the density profile flatter in the H-mode discharge (shown in Fig. 2) compared with the L-mode discharge (shown in Fig. 1). Also, the density at the edge of the H-mode plasma is much higher than the density at the edge of the L-mode plasma, relative to the line averaged density. This relatively high edge density is a characteristic of H-mode plasmas. In the BALDUR simulations, the shape of the density profile is a consequence of the self-consistent thermal and particle transport with the constraint that the density at the edge of the plasma is specified as a boundary condition, and the line averaged density is

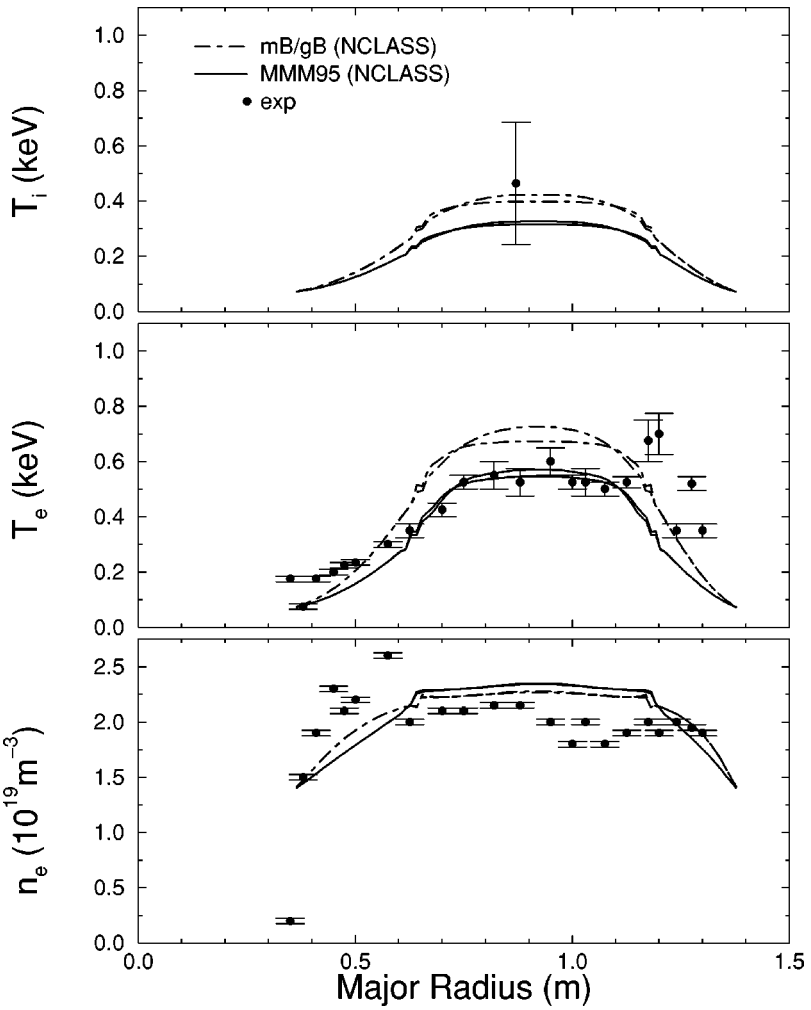

FIG. 2. Profiles of ion temperature, electron temperature, and electron density as a function of major radius for MAST discharge 2700 (*H*-mode) at 250 ms. Results obtained using the mB/gB model are plotted with a dashed curve while MMM95 results are plotted with a solid curve, with presawtooth crash (higher central temperature) and postsawtooth crash (lower central temperature). Experimental data are plotted as closed circles with error bars. NCLASS is used for neoclassical transport. The edge temperature is 0.07 keV.

controlled by gas puffing as a function of time. The boundary conditions used in the BALDUR simulation are taken from experimental data at the top of the pedestal that forms at the edge of *H*-mode plasmas. (The transport barrier that produces this edge pedestal is not included in these simulations.) Since *L*-mode plasmas are characterized by a relatively low edge density relative to the average density, these *L*-mode plasmas have relatively high recycling of ions at the edge, compared with *H*-mode plasmas. In the BALDUR simulations, the density is constantly replenished by gas puffing.

It is not known if the ion temperature profiles, predicted by the BALDUR code, are consistent with the experimental profiles since the experimental ion temperature profiles for the discharges considered are not available. Also, because a measurement of the edge ion temperature was not available, it is assumed in the simulations that the edge ion temperature, as a function of time, is the same as the edge electron temperature. The experimental central ion temperature deduced from the neutral particle analyzer data is 0.389 keV for the *L*-mode discharge and 0.464 keV for the *H*-mode discharge, as shown in the top panels of Figs. 1 and 2.

There is uncertainty in the temperature boundary value in the *H*-mode discharge since the experimental values for the inboard and the outboard edge temperatures differ. Given the uncertainty in edge temperature, simulations (using the MMM95 transport model) have been carried out with different boundary values for the temperature within the range of uncertainty indicated by the experimental data. The profile differences that result between a simulation using a relatively low edge temperature (0.07 keV) and one using a relatively high edge temperature (0.17 keV) are illustrated in Fig. 3. When the edge temperature is increased from 0.07 to 0.17 keV, the central electron temperature increases by approximately 25%. The increase in the core temperature, that results as the boundary temperature is increased, is partly an additive effect, but the effect is enhanced by the fact that the anomalous transport model is a function of the normalized temperature gradient.

The ion and electron temperature profiles result from the total transport, which includes contributions from anomalous as well as from neoclassical transport. Simulations have been carried out using two different neoclassical models, the NCLASS model or, alternatively, the Chang–Hinton (CH) model. Figure 4 illustrates the differences in the profiles that result when NCLASS is used in contrast to use of the Chang–Hinton model. It is found that the differences in the temperature profiles are typically small when changing from Chang–Hinton to NCLASS. The corresponding changes in the ion thermal model diffusivities are described in the following paragraphs.

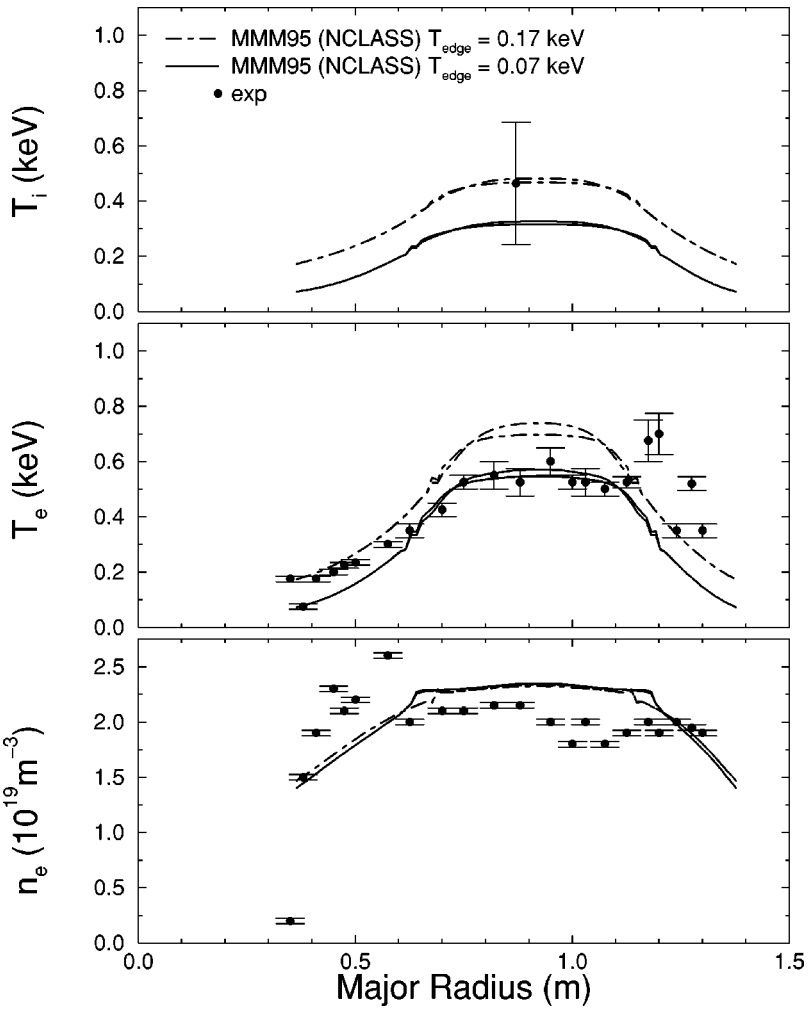

FIG. 3. Dependence of simulation profiles (obtained using the MMM95 and NCLASS transport models) on edge temperature. Profiles of ion temperature, electron temperature, and electron density are plotted as a function of major radius for MAST at 250 ms. Simulation results using an edge temperautre of 0.07 keV are plotted with a solid curve while results with an edge temperature of 0.17 keV, with a dashed curve. Simulation profies are those prior to a sawtooth crash. Experimental data are plotted as closed circles with error bars.

The ion thermal model diffusivities as a function of minor radius for the L-mode and the H-mode simulations are shown in Figs. 5 and 6, respectively. Almost all the ion thermal diffusivity in the inner third of the simulated plasma results from neoclassical transport. Similar results were found previously in the START spherical tokamak experiment.[13] In the following it is demonstrated that the relatively high value for the neoclassical transport predicted for the MAST H-mode discharge is roughly consistent with the scaled value for the neoclassical transport in a corresponding DIII-D discharge. Note that the spikes that appear in the thermal diffusivity in Figs. 5 and 6 are caused by localized peaks in the temperature and pressure gradient following each sawtooth crash. These spikes are localized and they have relatively little impact on the overall simulation results.

The neoclassical ion thermal diffusivity of the MAST H-mode discharge can be compared with a low density, low field, H-mode discharge in a conventional tokamak such as the DIII-D discharge 82 788. The neoclassical ion thermal diffusivity in discharge 82 788 ranges from about 0.1 to 2 m^2/s, with the highest values being in the very deep core and at the edge of the plasma. As an estimate of the scaling, we can write the ion thermal diffusivity as $\chi_i \propto \nu \rho_p^2$, where ν is the collision frequency, and ρ_p, the poloidal Larmor radius. In terms of the ion density, the poloidal magnetic field, and the temperature, this estimate of neoclassical ion thermal diffusivity χ_i scales as, $\chi_i \propto n_i/(B_\theta^2\sqrt{T})$ (i.e., $\nu \propto n_i/T^{3/2}$ and $\rho_p \propto T^{1/2}/B_\theta$). The ion density (edge deuterium density) and the poloidal magnetic field in discharge 82 788 are about 20% higher than those of the MAST H-mode discharge. The ion edge temperature of discharge 82 788 is 0.55 keV, compared with 0.07 keV for the MAST discharge. This scaling yields a neoclassical ion thermal diffusivity of about 7 m^2/s for the MAST H-mode discharge at the edge. This value is lower, although the same order of magnitude, as is observed in the MAST simulations. Near the edge of the plasma, the neoclassical and anomalous transport coefficients predicted by our models decrease with increasing temperature, stronger poloidal field, and lower collisionality. Thus, as the current in MAST is increased fourfold to its full design current of 2 MA, both the neoclassical and anomalous transport coefficients should decrease substantially (by an order of magnitude according to the simplified scaling estimates).

The beam heating profile for the L-mode and H-mode discharges simulated using the MMM95 anomalous transport model along with NCLASS are shown in Fig. 7. The highest energy of the fast ions produced by the neutral beam was 26.5 keV, which is high relative to the critical energy at

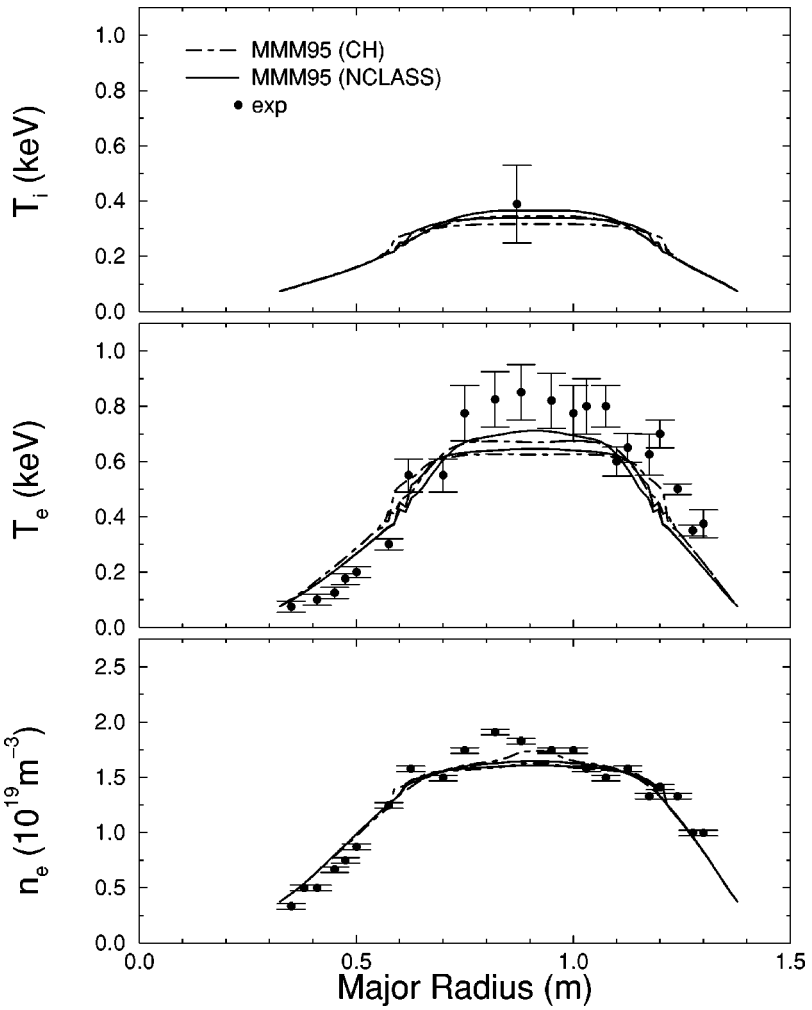

FIG. 4. Dependence of simulation profiles on choice of neoclassical model. Profiles of ion temperature, electron temperature, and electron density are shown as a function of major radius for MAST discharge 2701 (*L*-mode) at 250 ms. Results obtained using the NCLASS neoclassial model are plotted with a solid curve while results obtained using the Chang–Hinton (CH) model are plotted with a dashed curve. MMM95 is used for anomalous transport and the edge temperature is 0.07 keV in these simulations. The experimental data are plotted as closed circles with error bars.

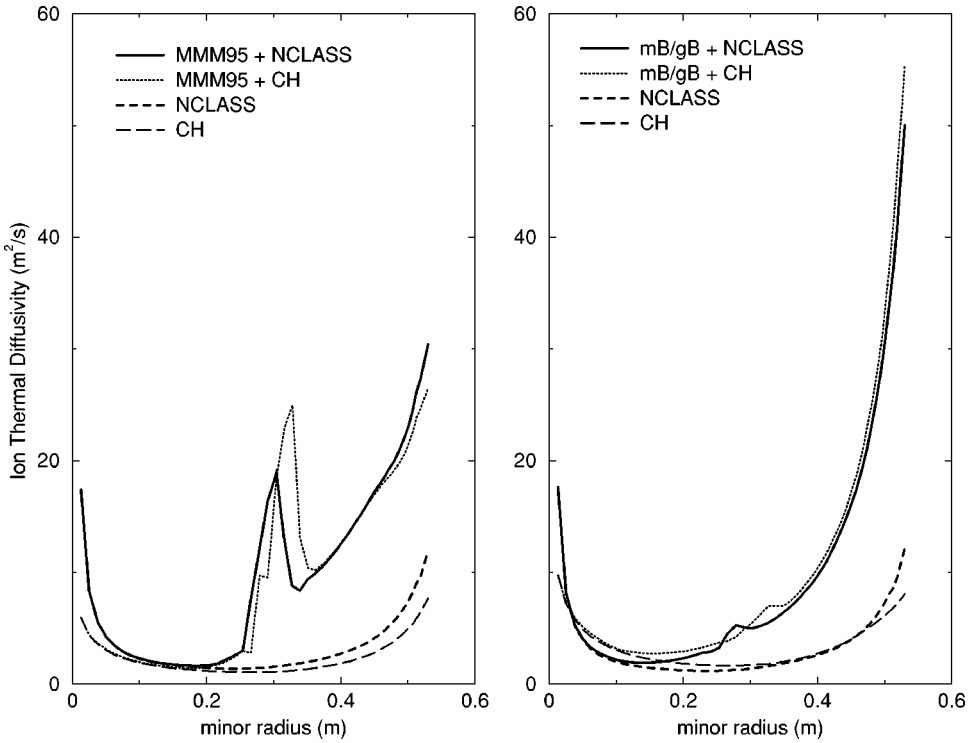

FIG. 5. The neoclassical and the total ion thermal diffusivities are plotted as a function of minor radius for simulations of MAST *L*-mode discharge 2701 with an edge temperature of 0.07 keV at 250 ms. Results are plotted in the left-hand panel using the MMM95 model together with NCLASS (solid line) or Chang–Hinton model (dot-dashed line). Corresponding results are plotted in the right-hand panel using the mB/gB anomalous transport model together with NCLASS or Chang–Hinton. The separate contributions to the diffusivities from the NCLASS (short dashes) or Chang–Hinton (long dashes) neoclassical models are also shown in each panel.

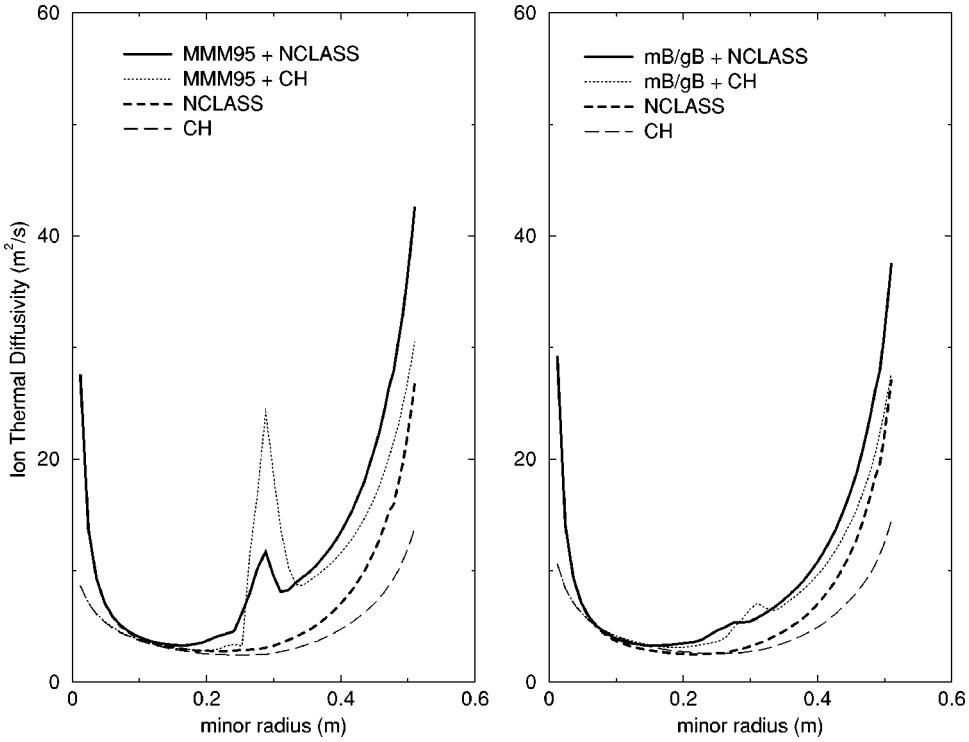

FIG. 6. The neoclassical and the total ion thermal diffusivities are plotted as a function of minor radius for simulations of MAST *H*-mode discharge 2700 with an edge temperature of 0.07 keV at 250 ms. Results are plotted in the left-hand panel using the MMM95 model together with NCLASS (solid line) or Chang–Hinton model (dot-dashed line). Corresponding results are plotted in the right-hand panel using the mB/gB anomalous transport model together with NCLASS or Chang–Hinton. The separate contributions to the diffusivities from the NCLASS (short dashes) or Chang–Hinton (long dashes) neoclassical models are also shown in each panel.

which the fast ion energy loss rate to background electrons and ions are equal during thermalization. Hence, more neutral beam power goes into heating thermal electrons than thermal ions. The energy of a fast neutral beam ion at which its rate of losing an equal amount of its energy to thermal electrons and thermal ions is approximately 5.5 keV in a plasma with $T_e \approx 0.6$ keV. For beam ions injected at the full energy (26.5 keV) and a background electron temperature of 0.6 keV, approximately two-thirds of the fast ion energy goes into heating thermal electrons and the remaining third goes into heating thermal ions.

The NBI heating profile extends from the magnetic axis out to about 50% of the plasma radius (about the same as the sawtooth mixing radius). When the sawteeth in the simulations are suppressed, the NBI heating profiles are found to be more narrow and peaked. The sharp drop in the heating pro-

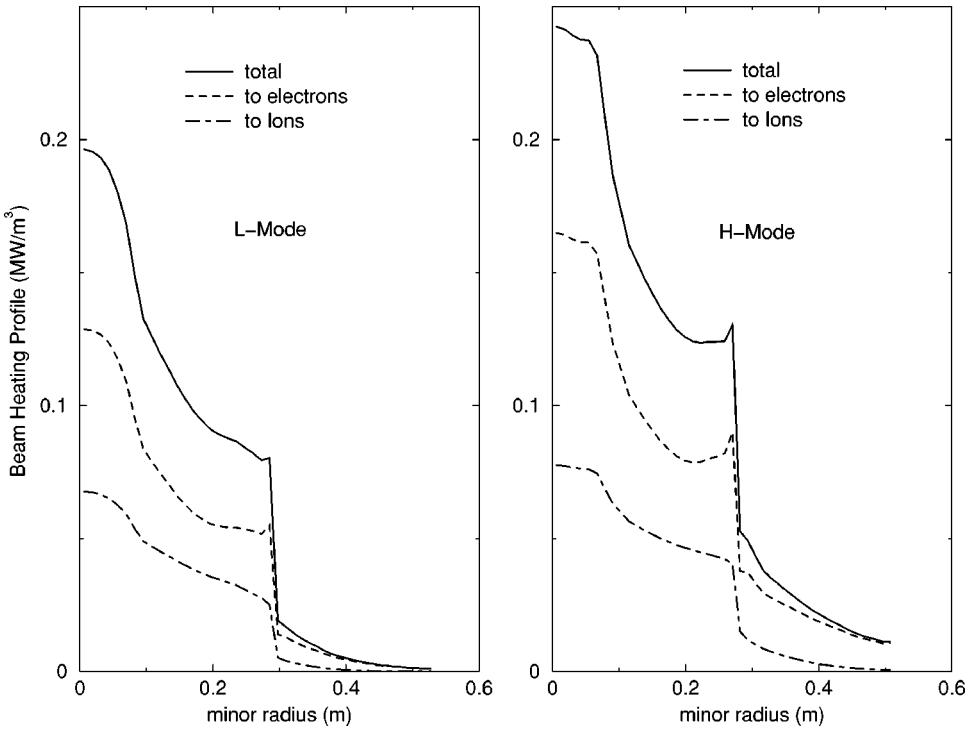

FIG. 7. The NBI ion heating profile (short dashed curve), the electron heating profile (long dashed curve), and the total heating profile (solid curve) are plotted as a function of minor radius from a simulation using the MMM95 anomalous transport model with NCLASS for neoclassical transport. The left-hand panel is for the *L*-mode discharge 2701, and the right-hand panel, for the *H*-mode discharge 2700. In both simulations, the edge temperature is 0.07 keV at 250 ms.

file in the vicinity of the mixing radius is a result of the mixing of the fast neutral beam ions during each sawtooth crash.

IV. SUMMARY

BALDUR simulations of a *L*-mode and *H*-mode MAST discharge are presented in this paper using either the mB/gB or the MMM95 anomalous transport models in addition to one of two neoclassical transport models. Sawtooth oscillations in the simulations have the effect of flattening the central temperature and density profiles as well as spreading the neutral beam injection heating across the broad radial sawtooth mixing region. Community efforts are under way to improve the model for the sawtooth period in order to produce better agreement with experimental data. The ion thermal diffusivity predicted by the simulations is close to neoclassical in the inner third of the plasma. This result is consistent with the experimental results previously reported for START.[13] The comparisons between BALDUR simulations and experimental data for the electron temperature and density profiles are shown in Figs. 1–4. The anomalous transport models used in these simulations appear to apply to low aspect ratio toroidal plasmas. However, the increased role of neoclassical transport in these plasmas may reduce the sensitivity of the simulation profiles to the choice of anomalous transport model. Although the major role played by neoclassical transport in these low-current discharges has reduced the sensitivity of the simulation profiles to the choice of anomalous transport model, this is not expected to be the case at higher plasma current, where neoclassical transport is expected to be much reduced.

ACKNOWLEDGMENTS

This work was supported by U.S. Department of Energy (DOE) under Contract No. DE-FG02-92-ER-5414. The MAST experiment is funded by EURATOM and the UK Department of Trade and Industry.

[1] A. Sykes, J. W. Ahn, R. Akers *et al.*, Phys. Plasmas **8**, 2101 (2001).
[2] A. Sykes, R. J. Akers, L. C. Appel *et al.*, Nucl. Fusion **41**, 1423 (2001).
[3] C. E. Singer, D. E. Post, D. R. Mikkelson *et al.*, Comput. Phys. Commun. **49**, 275 (1982).
[4] T. Onjun, G. Bateman, A. H. Kritz, and D. Hannum, Phys. Plasmas **8**, 975 (2001).
[5] D. Hannum, G. Bateman, J. Kinsey, A. H. Kritz, T. Onjun, and A. Pankin, Phys. Plasmas **8**, 964 (2001).
[6] G. Gennacchi and A. Taroni, in *Proceedings of the Eighth Europhysics Conference, Eibsee, 1986* (European Physical Society, Geneva, Switzerland, 1986), Computational Physics, Vol. 10D, p. 57.
[7] G. Bateman, A. H. Kritz, J. E. Kinsey, and A. J. Redd, Phys. Plasmas **5**, 1793 (1998).
[8] C. M. Roach, Plasma Phys. Controlled Fusion **38**, 2187 (1996).
[9] C. S. Chang and F. L. Hinton, Phys. Fluids **29**, 3314 (1986).
[10] W. A. Houlberg, K. C. Shaing, S. P. Hirshman, and M. C. Zarnstorff, Phys. Plasmas **4**, 3230 (1997).
[11] R. J. Hawryluk, S. Suckewer, and S. P. Hirshman, Nucl. Fusion **19**, 607 (1979).
[12] W. Park and D. Monticello, Nucl. Fusion **30**, 2413 (1990).
[13] C. M. Roach, R. J. Akers, N. J. Conway *et al.*, Nucl. Fusion **41**, 11 (2001).